Applied Surface Science 533 (2020) 147473

Contents lists available at ScienceDirect

Applied Surface Science

journal homepage: www.elsevier.com/locate/apsusc

Argon gas cluster fragmentation and scattering as a probe of the surface physics of thermoset polymers

Mykhailo Chundak[a,*], Claude Poleunis[a], Vincent Delmez[a], Hannah Jefford[a], Leila Bonnaud[b], Alain M. Jonas[a], Arnaud Delcorte[a]

[a] Institute of Condensed Matter and Nanosciences (IMCN), Université catholique de Louvain (UCL), Place Louis Pasteur 1, box L4.01.10 B-1348, Louvain-la-Neuve, Belgium

[b] Laboratory of Polymeric and Composite, Materials, Materia Nova Innovation Center in Materials of the University of Mons, 3 Avenue Nicolas Copernic, B-7000 Mons, Belgium

ARTICLE INFO

Keywords:
ToF SIMS
Ar clusters
Thermoset polymers
Thin films
Glass transition temperature

ABSTRACT

Surface and thin films are important in modern technologies and there is growing demand for their characterization. Secondary ion mass spectrometry (SIMS) is universally used for extracting information on the chemical composition of surfaces. This study shows that it can provide information about the physical (mechanical) properties of thermoset polymer surfaces. The intensities of backscattered Ar_n^+ clusters were measured upon 10 keV Ar_{3000}^+ gas cluster ion bombardment of polymer films. Tyrosol diaminodiphenylmethane based benzoxazine thermosets with different curing cycles were used. The intensity ratios $Ar_2^+/(Ar_2^+ + Ar_3^+)$ and $Ar_2^+/(Ar_2^+ + Ar_4^+)$ were highly sensitive to the physical changes of the thermoset coating surfaces as a function of their curing cycle and of temperature. These intensity ratios provide direct access to the surface transition temperature T_T (related to the bulk glass transition T_g), and show a dependence on the curing degree below and above T_T. Moreover, we discuss the influence of surface contamination and clusters induced roughness on the measured values. Our results suggest that contamination has a dramatic influence on the intensity of backscattered Ar_n^+ clusters, while that of roughness appears to be minor. This study constitutes a step forward towards a quantitative assessment of the mechanical properties of polymer coating surfaces using SIMS.

1. Introduction

Secondary ion mass spectrometry (SIMS) is considered as one of the most powerful techniques for surface chemical analysis and provides elemental, molecular and isotopic information about the sample, with nanometric depth resolution and submicron lateral resolution [1]. Nowadays, the most widespread experimental variant of SIMS is time-of-flight SIMS (ToF- SIMS), and development in this area is still ongoing. Among the latest improvements are large gas cluster ion beam (GCIB) sources which were introduced for SIMS analysis and depth-profiling [2]. Large clusters have several advantages over conventional single ions primary particles, as they can eject molecules from organic materials with minimum damage to the sample, due to the low kinetic energy per atom of the projectiles [3]. The majority of the secondary particles originate from the top nanometer of the bombarded surface, especially with large cluster ion bombardment [4], making it a highly surface sensitive characterization technique which is indispensable in some cases [1]. Thus, GCIBs have now become the reference ion source for the chemical and molecular analysis of organic coatings and films (organic electronics multilayers [5], cells and tissues [6]).

Owing to the outstanding surface sensitivity of GCIBs, researchers have proposed to use them to study mechanical properties of the materials, thin films and coatings. Until this day, such characterization was routinely done using the nanoindentation technique and peakforce quantitative nano-mechanical mapping (QNM). The nanoindentation method utilizes an indenter, which penetrates the sample with high precision control. The mechanical properties are derived directly from the load–displacement curve. The penetration depth is a critical parameter in the interpretation of the data as results can be highly influenced by the thickness of the films, interaction of the indenter with the material, effects of substrate and elastic properties of the coating. The peakforce QNM measurement uses the system that modulates z-piezo far below the resonance frequency and calculates very fast approach-retract curve for each pixel. Unlike the tapping mode Peak Force

* Corresponding author.
E-mail address: mykhailo.chundak@uclouvain.be (M. Chundak).

https://doi.org/10.1016/j.apsusc.2020.147473
Received 20 June 2020; Received in revised form 28 July 2020; Accepted 4 August 2020
Available online 07 August 2020
0169-4332/

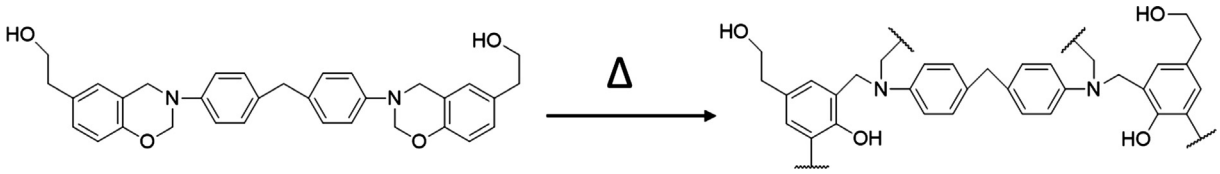

Fig. 1. Scheme of the benzoxazine monomer based on tyrosol and 4,4'-diaminodiphenylmethane (T-ddm) and its network after curing.

tapping controls the maximum force (Peak Force) on the tip enabling operation at lower forces than even what is achievable with normal tapping mode [7]. Hardness is a key property of the material and can be directly correlated with tensile strength. Twenty years from now, Insepov et al. [8] suggested to perform hardness measurements without indenter by gas-cluster beam bombardment. They found a correlation between sputtering yield, crater volume, clusters binding energy and hardness. This idea was developed by several other research groups [9,10]. Mochiji et al. [11] noticed that the decomposition of argon gas clusters on different metal surfaces varies. The Ar_n^+ cluster fragments were detected as a series of peaks in the secondary ion mass spectra, and the intensity ratio $Ar_2^+/\Sigma Ar_n^+$ ($n > 1$) was correlated to the calculated compressive stress induced upon impact. In their analytical model, the compressive stress was a function of the metal and the Ar_n^+ clusters mechanical properties (Young moduli, densities, velocity of the cluster). Thus, physical properties of the studied material could be uncovered by analyzing the intensity of the backscattered Ar_n^+ fragments. Generally speaking, a cluster dissociates more easily when the target is harder (i.e. more resistant to plastic deformation). Such an approach has a variety of advantages as it allows to avoid the interaction of an indenter with the surface and it enables the comparison of films with very different hardness values. Additionally, films down to tens of nanometers thickness can be studied and complementary information like chemical composition can be obtained. This idea was further developed in our lab and applied to model polymers [12]. According to the developed protocol we used the backscattered cluster ion ratios $Ar_2^+/(Ar_2^+ + Ar_3^+)$ and $Ar_2^+/(Ar_2^+ + Ar_4^+)$ to identify a pronounced and reproducible surface transition temperature (T_T) of polymers, which is related to the bulk glass transition temperature (T_g). The T_g is the point at which there is a sufficient free volume in the film to allow short macromolecular segments to move upon heating the polymer from the glass state [13]. Thus, transition of a polymer from a glassy state to the rubbery/viscous state occurs. T_g is crucially important for polymers as it dominates their temperature-dependent properties (including mechanical properties especially in the case of amorphous polymers) and thus their thermal range of applications. The T_g of polymer thin films in dependence on surface rearrangement of the films was previously studied by ToF SIMS and principal component analysis in [14,15]. However, these studies were done without utilization of backscattered ions gas clusters.

In this work we demonstrate that the protocol developed at our laboratory can be applied for thermoset polymers. More precisely, in this study, benzoxazine resins were used because they can be synthesized from renewable bio-sources and they display a series of beneficial properties, such as near-zero shrinkage, high T_g after curing, low water uptake, high char yield, excellent adhesion, etc [16]. These properties make benzoxazine resins desirable materials for a large number of applications including protective coatings for composite materials and metals used in the aerospace industry [17–23]. In particular for this work was selected a benzoxazine resin readily synthesized via the Mannich condensation reaction from tyrosol, a phenol derivative naturally present in olive leaves, diaminodiphenylmethane, a widely used amine of the polymer industry, and formaldehyde. More details about this resin can be found in the work of Horion [24]. Here, we demonstrate that the analysis of the backscattered Ar_n^+ cluster distribution allows us to follow the curing process of the thermoset polymer tyrosol 4,4'-diaminodiphenylmethane (T-ddm) and the associated change of T_T. It is shown that intensity ratios of the form $Ar_2^+/\Sigma Ar_n^+$ increase with the degree of cure below and above the transition temperature. Additionally, we elucidate the influence of the surface roughness and surface contamination on the intensity of the backscattered Ar_n^+ clusters. This work is a step forward towards understanding the fragmentation and backscattering of Ar_n^+ clusters upon impact, an approach which may help to overcome existing obstacles in measurements of mechanical properties of materials, nanomaterials, thin films and coatings.

2. Experimental

2.1. Samples

The benzoxazine precursors were supplied as a light-yellow powder by Materia Nova research center (Mons, Belgium). They were prepared in bulk directly from tyrosol, 4,4′-diaminodiphenylmethane and paraformaldehyde following a solventless procedure similar to the one first reported by Ishida et al [25]. The name of the resin T-ddm is given after the phenol and amine used for its preparation (respectively, T for tyrosol and ddm for 4,4′-diaminodiphenylmethane). The structure of T-ddm precursors are represented in Fig. 1. They can undergo ring-opening polymerization through thermal activation leading to the formation of a network as shown in Fig. 1. More precisely, T-ddm precursors exhibit a polymerization temperature of about 230 °C as determined by DSC (10 °C/min).

The benzoxazine powder was dissolved in dimethyl sulfoxide (DMSO) $(CH_3)_2SO$ which was supplied by Sigma-Aldrich Inc (Steinheim, Germany) with purity > 99.9%. The amount of 10 g T-ddm were dissolved in 100 mL of DMSO. The solution was then spin-coated onto clean Si wafers of 1 × 1 cm^2 area at 1000 rpm with acceleration 6000 rpm/s for 30 s. Before polymer deposition the Si wafers were sonicated in isopropanol and then dried under N_2 flux. The films were categorized into three groups: uncured (UC), half cured (HC) and fully cured (FC). After spin-coating the UC film was dried at 95 °C for 8 h, the HC film was heated at 165 °C for 60 min and the FC film was heated at 180 °C for 60 min and subsequently at 200 °C for 90 min. According to Differential Scanning Calorimetry (DSC, 10 °C/min), the UC films had $T_g \sim 40$ °C, the HC films $T_g \sim 113$ °C and the FC films $T_g \sim 165$ °C (Table 1). For the study of the sputtering yield volumes and the dependence of the Ar cluster fragmentation on the degree of cure at high and low temperature, two additional curing cycles were conducted on a new series of samples (150 °C for 60 min and 180 °C for 60 min).

DSC was conducted with an 821e Mettler Toledo in 40 μL aluminum pans. The measurements were performed under N_2 flow (50 mL/min)

Table 1
Curing conditions for the T-ddm benzoxazine samples, T_g measured by DSC and T_T measured with ToF SIMS along with the curing percentage derived from the DSC measurements.

Sample	Sample preparation conditions	Tg DSC (°C)	T_T ToF SIMS (°C)	α Degree of Cure %
UC	–	40 ± 0.2	55	0
HC	165 °C 60 min	113 ± 0.2	118	60
FC	165 °C 60 min + 200 °C 90 min	165 ± 0.2	~192	100

with an indium standard used for calibration with dynamic heating from 15 °C to 300 °C at 10 °C/min. The degree of curing α was found from reaction enthalpy ΔH using equation:

$$\alpha(\%) = \frac{\Delta H_{unc.} - \Delta H_{cur.}}{\Delta H_{unc.}} \times 100$$

where $\Delta H_{unc.}$ is the total enthalpy of reaction measured at certain heating rate for an uncured sample and $\Delta H_{cur.}$ is the residual heat of reaction for the isothermally cured sample for a certain period of time [26].

2.2. Morphology

To measure the morphology of the samples, an Atomic Force Microscope (AFM) Icon Dimension supplied by Bruker was used, with a tip PPP-NCHR-50 from NANOSENSORS. The measurements were performed in tapping mode. The scanning frames were 1 μm × 1 μm and 500 nm × 500 nm. The obtained AFM images were processed using the Gwyddion software [27]. The root mean square (RMS) roughness was calculated with a built-in tool from parallel line scans drawn across the images, and this 10 times per image, with a regular spacing between the lines. From these data, average values and standard deviations were determined. The reconstructed thickness of UC T-ddm film was c.a. 6 μm, of HC c.a. 4.4 μm and for FC sample 15 μm.

2.3. ToF-SIMS instrumentation

ToF-SIMS data were collected using a TOF.SIMS 5 apparatus (IONTOF GmbH, Münster, Germany). The instrument is equipped with an Ar gas cluster ion beam (Ar-GCIB) mounted at 45° with respect to the sample surface. It was used both as sputtering and analytical source. The time-of-flight mass analyzer is perpendicular to the sample surface. The Ar-GCIB ion source was operated at 10 keV and the cluster distribution was centered on Ar_{3000}^+.

For the spectral analyses, an AC target current of 0.0035 pA with a bunched pulse width around 70 ns was applied. A raster of 128 × 128 data points over an area of 500 × 500 μm^2 was utilized. The total primary ion beam dose per unit area for each analyzed region was kept below 8 × 10^{11} ions/cm^2. Only positive secondary ion species were analyzed. Mass resolution m/Δm ≈ 280 at 67 *m/z* (corresponding to $C_5H_7^+$) was maintained for spectral acquisition. Charge compensation was ensured using a very low energy electron flood gun (E_k = 20 eV). All the data analyses were carried out using the software supplied by the instrument manufacturer, SurfaceLab (ver. 6.5). Temperature was controlled with a special sample holder called "Holder G" (ION-TOF GmbH, Münster, Germany). This holder allows maintaining any temperature from −150 °C to +600 °C through a combination of simultaneous heating and cooling, with an accuracy of +/− 1 °C. The temperature was stabilized for 10 min before each measurement. Unless otherwise specified in the results, a pre-sputtering of 5 scans was performed before the start of the analysis with ToF-SIMS. Afterwards, 2 scans were added before each new measurement on the same area, whether at constant temperature or within heating and cooling cycles. The fluence of a single scan was 2 × 10^{12} Ar_{3000}^+/cm^2, over an area of 1 × 1 mm^2, and it was accumulated with the GCIB in DC mode. This procedure, carried out to eliminate the surface contaminations that occurred during the 10 min temperature stabilization, was recommended in [12].

3. Results and discussion

The possibility of derivation of the transition temperature T_T of benzoxazine thermosets by means of GCIB bombardment is demonstrated in Fig. 2. The plots use two different ratios of ion counts (or *breaking ratios* as they will be referred to in the remainder of the article) as a function of temperature, $Ar_2^+/(Ar_2^+ + Ar_3^+)$ in Fig. 2 a) and

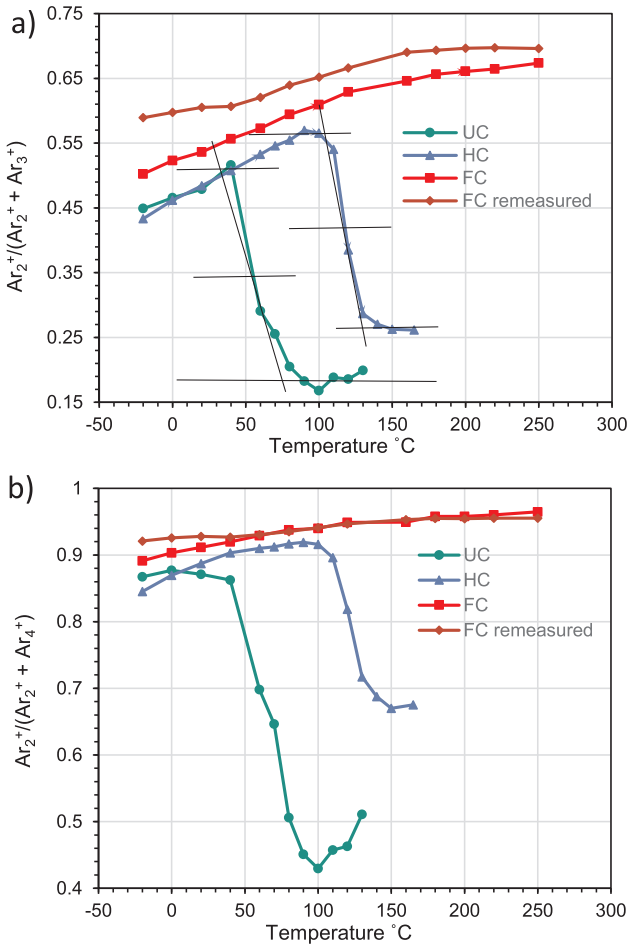

Fig. 2. Evolution of the breaking ratios as a function of temperature upon heating: a) $Ar_2^+/(Ar_2^+ + Ar_3^+)$ and b) $Ar_2^+/(Ar_2^+ + Ar_4^+)$ for T-ddm benzoxazine.

$Ar_2^+/(Ar_2^+ + Ar_4^+)$ in Fig. 2 b). These ratios were chosen because of the high intensities of Ar_2^+, Ar_3^+ and Ar_4^+ and negligible mass interference [12]. The T_T was derived from the plots of Fig. 2 by taking the temperature corresponding to 50% of the sharp decrease of the breaking ratios.

The measurements of T_T were performed on three samples with different curing cycles. For the UC sample, T_T was found to be ca. 55 °C while for the HC sample T_T ≈ 118 °C (Table 1). These values are sufficiently near the ones determined by DSC and they indicate that the protocol is suitable for thermoset polymers such as benzoxazine T-ddm. The reason why the measured T_T are slightly higher than the DSC values might be twofold: (i) the curing proceeds differently at the surface of the thin film (ToF-SIMS) and in the bulk (DSC); (ii) the different heating rates in the ToF-SIMS and the DSC leads to different degree of curing and/or different T_g values due to the dynamic nature of the glass transition. The heating rates in the ToF-SIMS is certainly influencing the results, as will be demonstrated later. As was mentioned in the experimental section, 10 min temperature stabilization periods are mandatory before every measurement, a period of time that might be sufficient for the crosslinking reaction to progress, depending on the temperature and free volume to equilibrate to different extents. This long stabilization time is absent in the DSC measurements, therefore there is no change in crosslinking prior to the measurement itself.

In the case of the FC sample, we did not detect a clear surface transition up to 250 °C. However, we saw change of the slope in breaking ratio values ~ 192 °C, this issue is discussed in more details in Section 3.2. Further heating was avoided, as it might cause charring of

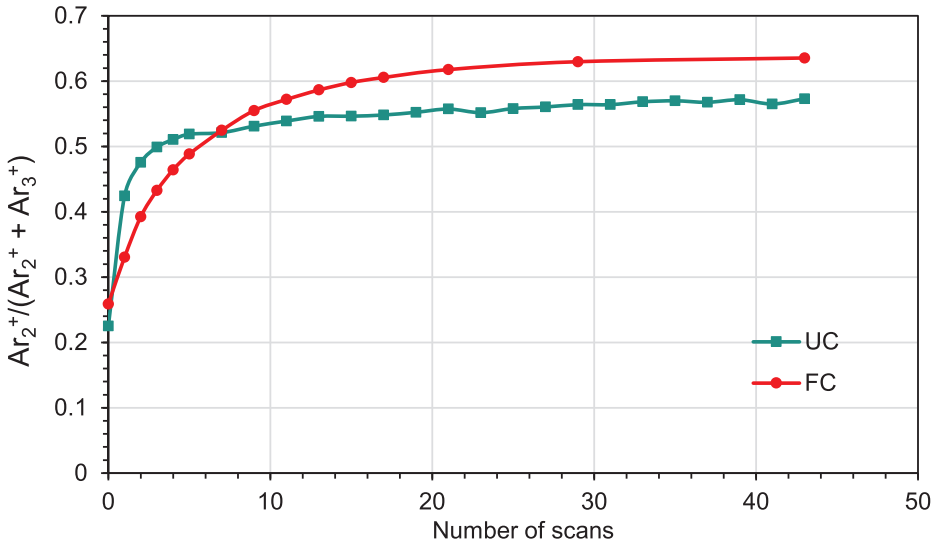

Fig. 3. Dependence of the breaking ratio $Ar_2^+/(Ar_2^+ + Ar_3^+)$ on the number of pre-sputtering scans, measured at room temperature for UC (green squares curve) and FC (red circles curve) samples. (For interpretation of the references to colour in this figure legend, the reader is referred to the web version of this article.)

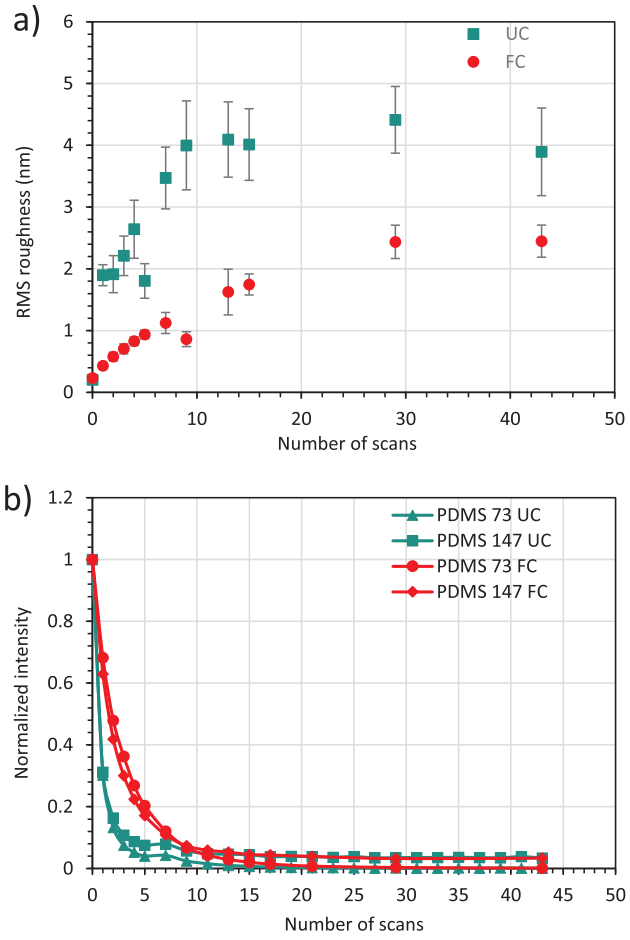

Fig. 4. Plots of the: a) RMS roughness evolution as a function of pre-sputtering scans, and b) Normalized intensity in the ToF-SIMS spectra of PDMS ions at 73 *m/z* and 147 *m/z* peaks, as a function of the number of pre-sputtering scans, measured at room temperature, for UC (green squares and triangles) and FC (red circles and diamonds) samples. (For interpretation of the references to colour in this figure legend, the reader is referred to the web version of this article.)

the T-ddm. Another puzzling observation is that, aside of the observed transitions, the values of breaking ratios tend to increase with temperature. This effect is more pronounced for the $Ar_2^+/(Ar_2^+ + Ar_3^+)$ breaking ratio. To test the influence of the pre-sputtering fluence on the measured ratio, the FC sample was measured a second time, with 15 scans of pre-sputtering instead of the 5 scans prescribed in the previously established protocol [12]. The measured values of the breaking ratios are consistently higher, and the value obtained at −20 °C in the second measurement is close to the one measured at 80 °C in the first measurement, i.e. with the same number of pre-sputtering scans Fig. 2a (dark red diamonds).

In order to better identify the cause of the effects observed in Fig. 2, the influence of pre-sputtering on the breaking ratios were first studied at room temperature. In the second part of the study, the effect of temperature is finally considered.

3.1. Effects of roughness and contamination at room temperature

The evolution of the breaking ratio $Ar_2^+/(Ar_2^+ + Ar_3^+)$ as a function of the number of sputtering scans is shown in Fig. 3 for the UC and FC films. The figure shows that the breaking ratio increases with the count of sputtering scans for both samples, but with a different dependence. The breaking ratio increases rapidly during 5 scans in the case of the UC sample (Fig. 3 green curve), then reaches a plateau, a dependence that justifies the protocol of Poleunis et al. [12], where 5 pre-sputtering scans were advised prior to any measurement. However, the plateau is not reached before 15 scans for the FC sample (Fig. 3 red circles). These different dynamics already suggest that the previous pre-sputtering protocol is not appropriate for all samples.

The related literature indicates that surface bombardment with energetic ions may induce two types of effects: chemical modifications (including defect creation, preferential sputtering, atomic mixing, etc.) and topography changes [28]. Because Ar cluster ions with a low energy per atom are known to preserve the molecular structure of sensitive organic and even biological samples, they are not expected to substantially modify the polymer surface by inducing chemical reactions [3,29]. Instead, we expect that the pre-sputtering gently desorbs the surface contaminants until a pristine polymer surface is uncovered. The effects of such a cluster ion bombardment on the local surface topography, however, might not be negligible. In turn, both the contaminant removal and the topography creation could influence the Ar_n^+ cluster ion fragmentation. Both of these aspects are investigated hereafter.

To assess the influence of the sputter cleaning on the roughness of the samples we performed a set of AFM measurements (Sup. Mat. Fig. 1 and Fig. 2). The results summarized in Fig. 4 a) demonstrate that the RMS roughness increases as a function of the sputtering scans for both the UC and the FC samples. After spin-coating from the DMSO solution and curing, the UC and FC samples have very smooth surfaces with RMS roughness $\approx 0.2 \pm 0.03$ nm and 0.23 ± 0.03 nm, respectively. In comparison, spin-coating from chloroform solutions failed to provide such smooth coatings because the solvent was evaporating too rapidly. With increasing sputtering fluence, the RMS roughness of the UC film increases rather quickly to reach a plateau value of $\sim$ 4 nm after 10 sputtering scans. In the case of the FC sample, the RMS roughness increases more gradually and finally reaches a plateau value of $\sim$ 2.4 nm after 30 sputtering scans. Immediately after 1 sputtering scan, one notices craters forming on the surface. For the UC sample, the smallest crater diameters are approximately $\sim$ 20 nm with the rim up to 3 nm in height. In contrast, for the FC sample, the crater diameters are up to 7 nm and the rims are up to 1.2 nm in height. This indicates that the displacement of the material is more pronounced at the surface of the UC sample each time a crater is created, which in turn explains a faster increase of roughness as a function of the sputtering scans. In support of this estimation is the sputtering yield volume which was found for the UC sample to be $Y = 28.2$ nm^3 and for FC sample $Y = 10.4$ nm^3.

Simultaneously with the topography development, the chemical nature of the surface is easily assessed by the change in the secondary ion mass spectra as a function of the sputtering fluence. The intensities of the peaks in the mass spectra vary significantly at the beginning of the experiments. As an example, Fig. 4 b) shows the evolution of the relative intensities of two fragment ions (m/z 73 and 147) of the ubiquitous contaminant, polydimethylsiloxane (PDMS), for the UC and FC samples. In Fig. 4 b), the peak intensities are divided by the total intensity of the mass spectra and then divided by the maximum value. For the UC sample, the PDMS peak intensities decrease rapidly from 0 to 5 scans and become negligible after 10 scans. In the case of the FC sample, the decay is slower and the signals become negligible after 15 scans only.

The breaking ratio is a ratio of different Ar_n^+ ions, so for a better understanding of how the contaminants and roughness influence these ions, the Ar_n^+ ($n \leq 4$) ion intensities are plotted as a function of these two parameters in Fig. 5. In Fig. 5 a), c), the intensity of the Ar_n^+ ions is represented as a function of the intensity of the PDMS fragment ion at $m/z = 147$ for the UC and FC samples, respectively. For the UC sample (Fig. 5 a)), the Ar_2^+ ion intensity has small variations in the values, while the Ar_3^+ and Ar_4^+ intensities increase linearly with the PDMS ion intensity. The equations (on the plot) determine the best linear fit, with R^2 values demonstrating good correlations between the $Ar_{3\text{-}4}^+$ cluster intensities and the PDMS ion intensity. Such linear correlations (or anti-correlations) cannot be found between the Ar_n^+ ions clusters intensities and the sample roughness (Fig. 5 b)), suggesting thus that the influence of roughness on the Ar_n^+ ions intensities is not the prevalent effect. In Fig. 5 c) positive correlations between the $Ar_{3\text{-}4}^+$ cluster intensities and the contaminant intensities are also found for the FC sample, whereas Ar_2^+ tends to increase slightly while the contamination is removed. The same sort of correlations can be drawn with other contamination peaks, which follow similar dependencies on the bombardment fluence as the considered PDMS peak (data not shown). For both the FC and the UC sample, positive linear correlations between the roughness and the Ar_n^+ ion intensities can never be found. For both samples, the atomic ion Ar^+ intensity increases largely while removing the contamination.

All the samples, including the UC film, are below their surface transition at room temperature, i.e. their molecular segments are less mobile and their surface is more solid than liquid-like (harder in macroscopic terms). Our interpretation is that the contamination layer forms a softer, liquid-like layer at the surface of the samples. Upon removal of the contamination by sputtering, the surface evolves from a soft layer to a harder material, and the impinging clusters fragment more extensively. This results in a gradual decrease of the larger cluster intensities and an increase of the monoatomic ion intensities. This interpretation is similar to the one used to describe the strong variation of Ar_n^+ ion intensities during polymers transitions between the glassy and the rubbery state [12]. Linear correlations could then be explained by the fact that the effect is proportional to the fraction of the surface area that is covered by contaminants, assuming that this coverage is less than a monolayer. Though the intensity of the contaminants (PDMS) is drastically reduced (2 orders of magnitude in intensity), Fig. 5 a), c) and Fig. 4 b) show that it does not level off completely, indicating that a fraction of the contaminants also diffused into the film. This diffusion occurs most probably during the drying and the curing step of the sample preparation.

Roughness does not appear to be the dominant factor in the explanation of the Ar cluster projectile fragmentation. Nevertheless, because contamination removal necessarily involves pre-sputtering and therefore topography creation, the two effects cannot be decoupled and the influence of roughness cannot be fully discarded. In the literature, the influence of roughness on the SIMS intensities has been reported, for instance, in the case of micrometer size topography [30,31]. The ion intensities depend not only on the surface composition, but also on the surface morphology height and inclination with respect to the incident beam. An increase of roughness should also tend to increase large cluster projectile fragmentation, as was indicated by recent simulations of CO_2 cluster impacts on flat and rough samples [32]. However, the case of Fig. 5 b) shows that the Ar_n^+ intensities stabilize quite rapidly, while the RMS roughness continues to increase strongly, beyond 1 nm. In addition, comparing Fig. 5 b) and 5 d), all the curves are shifted to a value of RMS roughness that is smaller by a factor of two, on average, when going from the UC to the FC material, which is, once again, not consistent with a dominant influence of topography in the observed evolutions.

3.2. Effects of temperature

Fig. 2 shows that the breaking ratios tend to increase with increasing temperature before the T_T. It is particularly obvious for the UC sample, as was mentioned earlier in this article. However, we showed in Section 3.1 that at least a part of the data of Fig. 2 was affected by the inherent variation of the breaking ratios in the beginning of the experiment, before the evolution of the backscattered Ar_n^+ ion intensities reach a steady-state. This is consistent with the shift of the $Ar_2^+/(Ar_2^+ + Ar_3^+)$ breaking ratio for the FC sample, when 15 pre-sputtering scans are conducted instead of 5 (Fig. 2).

In order to avoid the interference with transient effects, mentioned in the paragraph above, the Ar_n^+ ions intensities were analyzed upon cooling the samples after the first heating cycle. In general, this approach should not be recommended to estimate the T_T for such thermosets if they are not fully cured, because the first heating cycle allows the crosslinking reaction to progress, leading to a shift of the transition towards higher temperatures. However, it seems reasonable to investigate the effect of temperature on the breaking ratio, especially for the FC sample, which does not exhibit a transition below T_T and should not evolve anymore upon thermal cycling. In the case of FC sample, we observe the slight change of the breaking ratio slope after $\sim$ 150 °C (Sup. Mat. Fig. 3), but due to the reasons of degradation of the material above 250 °C, the exact T_T could not be established. Nevertheless similar change of the breaking ratio slope was seen for T-ddm sample spin coated with chloroform as solvent (Sup. Mat. Fig. 3). Thus, it is reasonable to tentatively assign $T_T \sim 192$ °C as demonstrated in Table 1. And the breaking ratio curve under the T_T can be used for analysis of the temperature influence.

The intensities of the Ar_n^+ ions obtained upon sample cooling are reported in Fig. 6 as a function of temperature. These data clearly demonstrate that there is a linear correlation between the Ar_n^+ ions

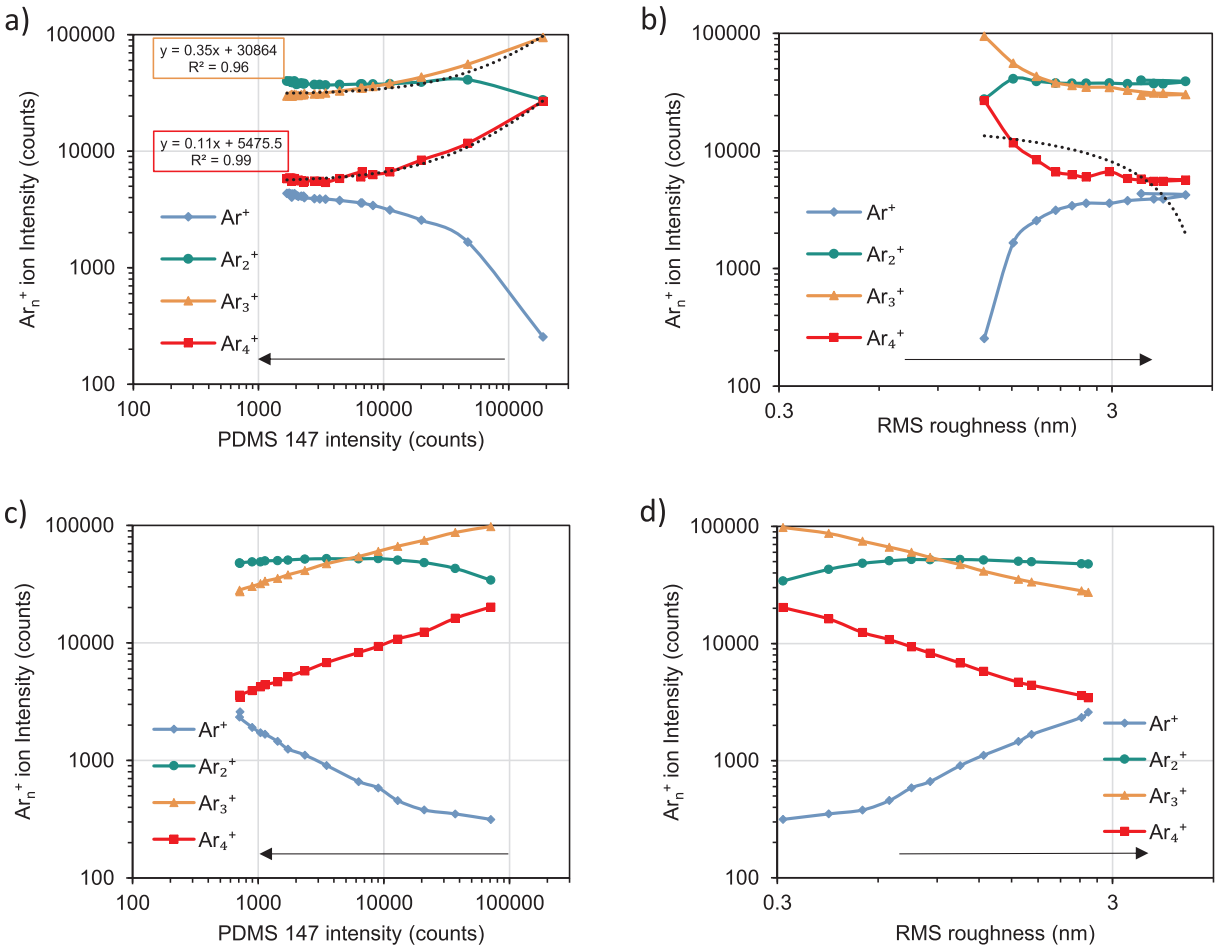

Fig. 5. Plots of the absolute intensities of the Ar_n^+ ions in the ToF-SIMS spectra as a function of the absolute intensities of the PDMS ion at *m/z* 147 and the RMS roughness for the UC: a), b) and the FC samples: c), d). Some of the curves in a) and b) are fit with linear regressions (dotted lines) for illustration (Equations in colored frames, where R^2 is the coefficient of determination). The arrows indicate the direction of sputtering time.

intensities and the temperature, and here it is not caused by a variation of the contaminations or roughness during the transient phase. Interestingly, the extrapolations of the linear fit of the Ar_n^+ (n = 2–4) cluster intensities all have an intercept with the x-axis in the −160 to −180 °C range.

The fact that all the Ar_n^+ ion intensities tend to zero with decreasing temperature points to an effect of ionization and/or neutralization. Indeed, the impinging clusters have ~ 3 eV/atom of translational energy, which is largely transformed into internal energy upon impact. This energy is much larger than any thermal energy provided by the substrate and, therefore, the colliding cluster should fragment into small clusters and atoms even at 0 K, as indicated by molecular dynamics simulations [4]. Beside fragmentation, an ionization probability change should then be the next logical cause of these variations. A detailed investigation of this effect would require experiments with other surfaces and cluster beams (Ne, Kr), which is outside the scope of this work. Nevertheless, we note that a test of the temperature dependence of the backscattered Ar_n^+ ion intensities for clean silicon surfaces does not show a trend similar to Fig. 6. Instead, the Ar_n^+ ion intensities remain almost constant in between −20 and 250 °C (See Sup. Mat. Figs. 4, 5).

Even though the data reported in Fig. 6 show a clear temperature dependence of the backscattered Ar_n^+ absolute intensities, those are linear and with a very close intercept with the x-axis for $Ar_{2\text{-}4}^+$. Therefore, the breaking ratios $Ar_2^+/(Ar_2^+ + Ar_3^+)$ and $Ar_2^+/(Ar_2^+ + Ar_4^+)$ should be considered constant over the whole examined temperature range up to the T_T, within the experimental uncertainty.

The curves of the breaking ratios obtained upon cooling for the UC, HC and FC samples are displayed in Fig. 7 (shown as a dashed lines).

Upon cooling, the T_T of the UC sample moved to a higher temperature. This can be explained by the continuation of the curing reaction during the sample heating. In the case of the HC sample no change of T_T was seen, probably due to the slowing down of the curing reaction since it already took place during the preparation of the sample. Further reaction would require heating to higher temperatures. Fig. 7 a), b) demonstrate that after cooling the breaking ratios return to higher values. These data clearly show that additional cleaning of the surface is needed before measurements to obtain proper values.

The curves of Fig. 7 are reminiscent of the curves measured with the techniques of dynamic-mechanical measurement [33] and torsional braid for polymers [34]. Those latter curves show that the higher the crosslinking degree of the thermoset, the higher the T_g of the material, as well as its modulus and hardness above T_g, which is a well-known phenomenon [35]. In line with Mochiji et al. [11], our interpretation of the breaking ratio variations at T_T is also based on the change of the physical and mechanical properties of the surface [12]. The curves of Fig. 7 also indicate an increase of the breaking ratio as a function of the curing degree (and thus the crosslinking) for the T-ddm benzoxazine, both above and below the transition temperature. In order to confirm this trend, two additional samples with respectively ~ 40% and ~ 90% cure (as determined from DSC) were analyzed. In this case, only one heating cycle was performed, but with a long period of pre-sputtering (20 scans), in order to remove contamination. Our results obtained with these additional samples (See Sup. Mat. Fig. 6) confirm that the

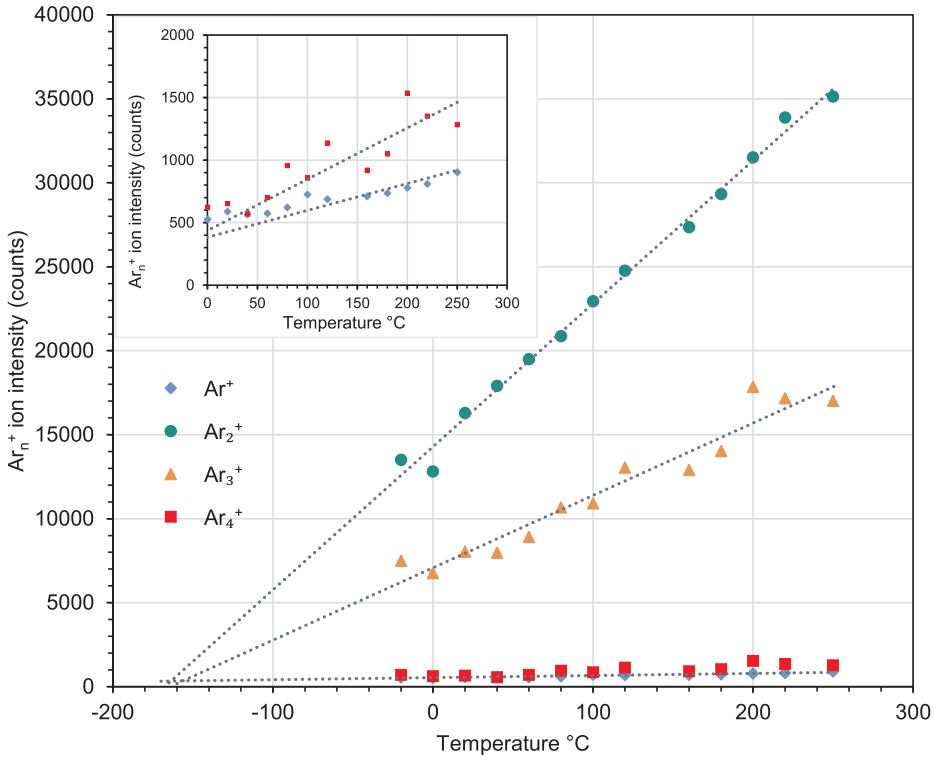

Fig. 6. Dependences of the absolute intensities of the Ar_n^+ ions in the ToF-SIMS spectra on temperature for the FC sample (cooling part of the thermal cycle). *Inset:* zoom on the Ar^+ and Ar_4^+ ion intensities.

breaking ratios generally increase with the crosslinking degree, both under T_T and above, as shown in Table 2. Interestingly, this increase is very clear above T_T, in line with the increase of modulus reported in the literature above T_g. Thus, our new results are consistent with the idea that the breaking ratios as shown in Fig. 7 are directly related to the mechanical properties of the material.

4. Conclusion

Since GCIBs have been applied for soft sputtering in SIMS, new dimensions of surface and thin film analysis have emerged, such as molecular depth profiling and 3D molecular imaging of organic and biological samples. It was also shown that information could be obtained from the backscattering of the ionized projectile fragments, observed in the mass spectra. In this article, we used the information contained in the backscattered cluster fragment ion distributions to probe the surface transition temperature T_T (related to bulk T_g) of polymers. Our results show that this approach, recently proposed for commercial thermoplastics such as PS and PMMA, can be applied to more complex thermoset polymers. The surface of the T-ddm benzoxazine thin films with different crosslinking degrees (different curing cycles) was bombarded by 10 keV Ar_{3000}^+ and the generated ion distributions were measured with a time-of-flight mass spectrometer. The temperature dependence of the breaking ratios $Ar_2^+/(Ar_2^+ + Ar_3^+)$ and $Ar_2^+/(Ar_2^+ + Ar_4^+)$ clearly indicate a transition temperature T_T, increasing with the crosslinking degree. To improve the protocol, we studied the influences of surface contamination, surface roughness and temperature changes on the breaking ratios. The obtained data allow us to conclude that surface contamination has a major influence on the measured values, while that of surface roughness is secondary. Thus, a careful surface cleaning procedure should be established for each sample individually. A detailed analysis of the data obtained on the fully cured sample shows that the backscattered Ar_n^+ ion intensities increase linearly with temperature in the investigated range, but this variation cancels out in the breaking ratios. The temperature dependences of the breaking ratios are reminiscent of dynamic-mechanical and torsional braid measurements, confirming again the link of the cluster fragmentation with the surface physics. The next step of this research will be to establish quantitative relationships between the backscattered Ar_n^+ ion intensities measured with ToF-SIMS and the physical properties of organic surfaces.

CRediT authorship contribution statement

Mykhailo Chundak: Conceptualization, Methodology, Formal analysis, Investigation, Validation, Writing - original draft, Visualization, Supervision, Project administration. **Claude Poleunis:** Resources, Investigation. **Vincent Delmez:** Investigation, Formal analysis. **Hannah Jefford:** Investigation, Formal analysis. **Leila Bonnaud:** Resources, Validation. **Alain M. Jonas:** Methodology, Validation. **Arnaud Delcorte:** Conceptualization, Methodology, Validation, Formal analysis, Resources, Visualization, Supervision, Project administration, Funding acquisition.

Declaration of Competing Interest

The authors declare that they have no known competing financial interests or personal relationships that could have appeared to influence the work reported in this paper.

Acknowledgment

M.C. would like to acknowledge the “Fonds National de la Recherche Scientifique” (FNRS), Belgium for financing the project CLUSTERPROBE under the convention PDR T.0065.18. A.D. is a Research Director of FNRS. Dr. K. Moshkunov is gratefully acknowledged for insightful scientific discussions. L.B. wishes to thank Wallonie and the European Community for general support in the framework of the Interreg V FWVL program (“BIOCOMPAL” and “ATHENS” projects)

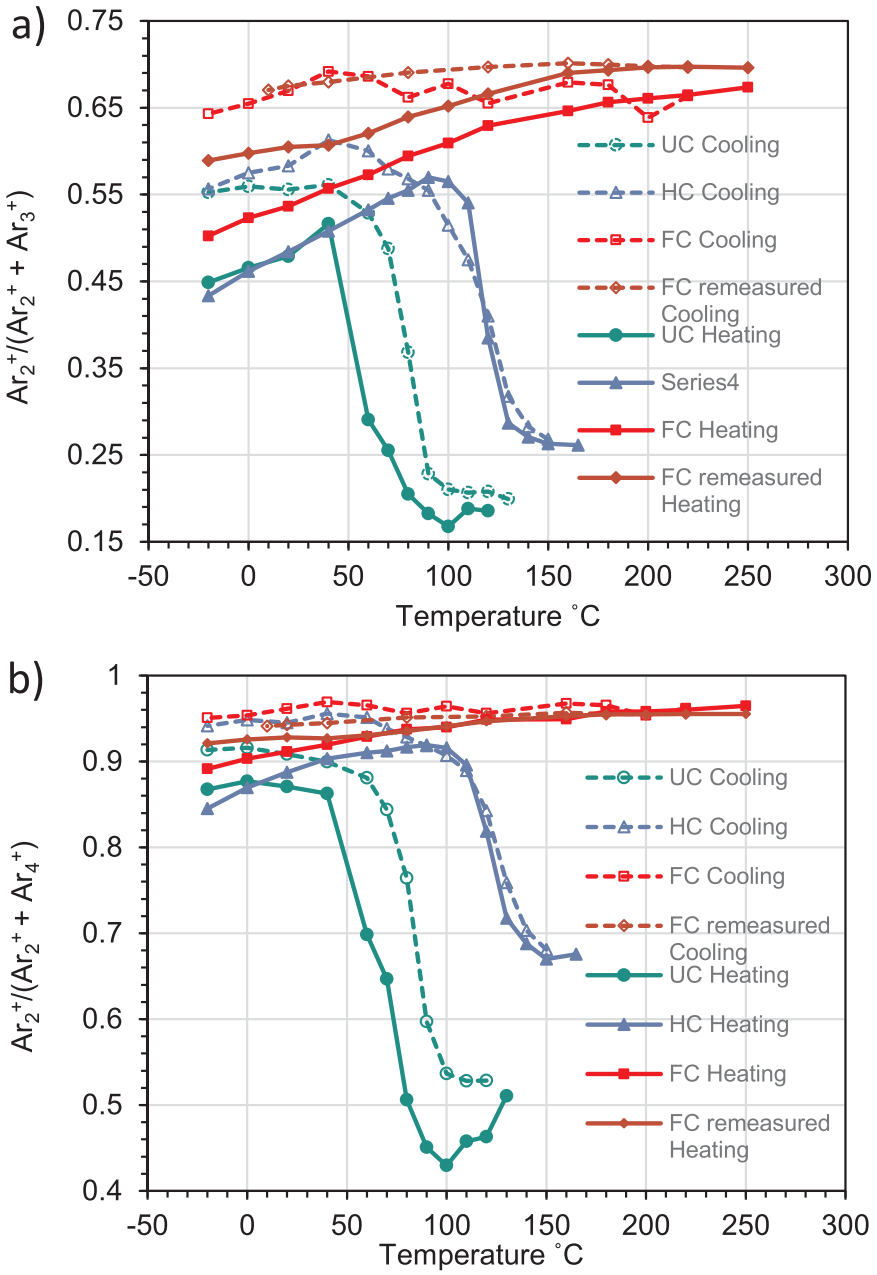

Fig. 7. Temperature dependence of the breaking ratios upon heating (full lines) and cooling (dashed line): a) $Ar_2^+/(Ar_2^+ + Ar_3^+)$ and b) $Ar_2^+/(Ar_2^+ + Ar_4^+)$ for T-ddm benzoxazine samples.

Table 2
Values of the sputter yield volumes, transition temperatures (T_T) and breaking ratios $Ar_2^+/(Ar_2^+ + Ar_3^+)$ and $Ar_2^+/(Ar_2^+ + Ar_4^+)$ below and above T_T as a function of the degree of cure (%) for T-ddm benzoxazine. The value for UC sample with no heating is for the sample without thermal treatment.

α Degree of Cure %	T_T ToF SIMS (°C)	Sputter yield volume (nm^3)	$Ar_2^+/(Ar_2^+ + Ar_3^+)$ below T_T	$Ar_2^+/(Ar_2^+ + Ar_3^+)$ above T_T	$Ar_2^+/(Ar_2^+ + Ar_4^+)$ below T_T	$Ar_2^+/(Ar_2^+ + Ar_4^+)$ above T_T
0	55	28.2 (47.3 with no heating)	0.52	0.2	0.9	0.47
40	92	19.2	0.54	0.25	0.86	0.64
60	118	14.8	0.59	0.27	0.93	0.68
90	159	10.6	0.62	0.34	0.94	0.78
100	~192	10.4	0.7	–	0.95	–

Appendix A. Supplementary data

Supplementary data to this article can be found online at https://doi.org/10.1016/j.apsusc.2020.147473.

References

[1] J.C. Vickerman, D. Briggs, TOF-SIMS materials analysis by mass spectrometry, 2nd edition, IM Publications and SurfaceSpectra Limited, Manchester, 2013.

[2] S. Ninomiya, K. Ichiki, Y. Nakata, Y. Honda, T. Seki, T. Aoki, J. Matsuo, Secondary ion emission from Si bombarded with large Ar cluster ions under UHV conditions, Appl. Surf. Sci. 255 (2008) 880–882, https://doi.org/10.1016/j.apsusc.2008.05.063.

[3] A. Delcorte, V. Cristaudo, V. Lebec, B. Czerwinski, Sputtering of polymers by keV clusters: Microscopic views of the molecular dynamics, Int. J. Mass Spectrom. 370 (2014) 29–38, https://doi.org/10.1016/j.ijms.2014.06.017.

[4] A. Delcorte, M. Debongnie, Macromolecular sample sputtering by large Ar and CH_4 clusters: elucidating chain size and projectile effects with molecular dynamics, The Journal of Physical Chemistry C 119 (2015) 25868–25879, https://doi.org/10.1021/acs.jpcc.5b07007.

[5] T. Mouhib, C. Poleunis, N. Wehbe, J.J. Michels, Y. Galagan, L. Houssiau, P. Bertrand, A. Delcorte, Molecular depth profiling of organic photovoltaic heterojunction layers by ToF-SIMS: comparative evaluation of three sputtering beams, Analyst 138 (2013) 6801–6810, https://doi.org/10.1039/C3AN01035J.

[6] J.S. Fletcher, S. Rabbani, A.M. Barber, N.P. Lockyer, J.C. Vickerman, Comparison of C_{60} and GCIB primary ion beams for the analysis of cancer cells and tumour sections, Surf. Interface Anal. 45 (2013) 273–276, https://doi.org/10.1002/sia.4874.

[7] B. Pittenger, N. Erina, C. Su, Quantitative mechanical property mapping at the nanoscale with PeakForce QNM, Application Note Veeco Instruments Inc, 1 (2010) 1-11.

[8] Z. Insepov, R. Manory, J. Matsuo, I. Yamada, Proposal for a hardness measurement technique without indentor by gas-cluster-beam bombardment, Physical Review B 61 (2000) 8744–8752, https://doi.org/10.1103/PhysRevB.61.8744.

[9] N. Toyoda, Development of non-contact hardness measurements with crater formations by gas cluster ions, in: 2016 IEEE 16th International Conference on Nanotechnology (IEEE-NANO), 2016, pp. 381–382, , https://doi.org/10.1109/NANO.2016.7751355.

[10] E. Onorati, E. Iacob, R. Bartali, M. Barozzi, S. Gennaro, M. Bersani, Experimental study by Secondary Ion Mass Spectrometry focused on the relationship between hardness and sputtering rate in hard coatings, Thin Solid Films 625 (2017) 35–41, https://doi.org/10.1016/j.tsf.2017.01.038.

[11] K. Mochiji, N. Se, N. Inui, K. Moritani, Mass spectrometric analysis of the dissociation of argon cluster ions in collision with several kinds of metal, Rapid Commun. Mass Spectrom. 28 (2014) 2141–2146, https://doi.org/10.1002/rcm.7004.

[12] C. Poleunis, V. Cristaudo, A. Delcorte, Temperature dependence of Ar_n^+ cluster backscattering from polymer surfaces: a new method to determine the surface glass transition temperature, J. Am. Soc. Mass Spectrom. 29 (2018) 4–7, https://doi.org/10.1021/jasms.8b05678.

[13] P.C. Painter, M.M. Coleman, Fundamentals of polymer science an introductory text, Technomic Publishing Company Inc, Lancaster, US, 1994.

[14] Y. Fu, Y.-T.R. Lau, L.-T. Weng, K.-M. Ng, C.-M. Chan, Evidence of enhanced mobility at the free surface of supported polymer films by in situ variable-temperature time-of-flight-secondary ion mass spectrometry, Anal. Chem. 85 (2013) 10725–10732, https://doi.org/10.1021/ac401335j.

[15] Y. Fu, Y.-T.R. Lau, L.-T. Weng, K.-M. Ng, C.-M. Chan, Transition temperature of poly (methyl methacrylate) determined by time-of-flight secondary ion mass spectrometry and contact angle measurements, J. Colloid Interface Sci. 504 (2017) 758–764, https://doi.org/10.1016/j.jcis.2017.05.120.

[16] H. Ishida, T. Agag, Handbook of Benzoxazine Resins, Elsevier, Amsterdam, 2011.

[17] J. Escobar, M. Poorteman, L. Dumas, L. Bonnaud, P. Dubois, M.-G. Olivier, Thermal curing study of bisphenol A benzoxazine for barrier coating applications on 1050 aluminum alloy, Prog. Org. Coat. 79 (2015) 53–61, https://doi.org/10.1016/j.porgcoat.2014.11.004.

[18] E. Pospisilova, A. Renaud, M. Poorteman, M. Olivier, L. Dumas, P. Dubois, L. Bonnaud, K. Moshkunov, B. Nysten, A. Delcorte, A quantitative determination of the polymerization of benzoxazine thin coatings by time-of-flight secondary ion mass spectrometry, Surf. Interface Anal. 51 (2019) 674–680, https://doi.org/10.1002/sia.6639.

[19] T. Zhang, L. Bonnaud, J.-M. Raquez, M. Poorteman, M. Olivier, P. Dubois, Cerium salts: an efficient curing catalyst for benzoxazine based coatings, Polymers 12 (2020) 415, https://doi.org/10.3390/polym12020415.

[20] A. Renaud, Y. Paint, A. Lanzutti, L. Bonnaud, L. Fedrizzi, P. Dubois, M. Poorteman, M.-G. Olivier, Sealing porous anodic layers on AA2024-T3 with a low viscosity benzoxazine resin for corrosion protection in aeronautical applications, RSC Adv. 9 (2019) 16819–16830, https://doi.org/10.1039/C9RA01970G.

[21] L. Dumas, L. Bonnaud, M. Olivier, M. Poorteman, P. Dubois, Multiscale benzoxazine composites: The role of pristine CNTs as efficient reinforcing agents for high-performance applications, Compos. B Eng. 112 (2017) 57–65, https://doi.org/10.1016/j.compositesb.2016.12.039.

[22] A. Renaud, M. Poorteman, J. Escobar, L. Dumas, Y. Paint, L. Bonnaud, P. Dubois, M.-G. Olivier, A new corrosion protection approach for aeronautical applications combining a Phenol-paraPhenyleneDiAmine benzoxazine resin applied on sulfo-tartaric anodized aluminum, Prog. Org. Coat. 112 (2017) 278–287, https://doi.org/10.1016/j.porgcoat.2017.07.007.

[23] F. Samyn, O. Murariu, L. Bonnaud, S. Duquesne, Preparation and flame retardancy of flax fabric/polybenzoxazine laminates, Fire Mater. (2020) 1–13, https://doi.org/10.1002/fam.2839.

[24] J. Horion, Nanocomposites from novel polybenzoxazines, in, Université Catholique de Louvain, Louvain-La-Neuve, 2019.

[25] H. Ishida, Process for preparation of benzoxazine compounds in solventless systems, in, US (1996).

[26] R. Hardis, J.L.P. Jessop, F.E. Peters, M.R. Kessler, Cure kinetics characterization and monitoring of an epoxy resin using DSC, Raman spectroscopy, and DEA, Compos. A Appl. Sci. Manuf. 49 (2013) 100–108, https://doi.org/10.1016/j.compositesa.2013.01.021.

[27] N. David, K. Petr, Gwyddion: an open-source software for SPM data analysis, Open Physics 10 (2012) 181–188, https://doi.org/10.2478/s11534-011-0096-2.

[28] C.M. Mahoney, Cluster secondary ion mass spectrometry of polymers and related materials, Mass Spectrom. Rev. 29 (2010) 247–293, https://doi.org/10.1002/mas.20233.

[29] A. Delcorte, C. Poleunis, Mechanistic insight into gas cluster-induced sputtering of kilodalton molecules using kinetic energy distribution measurements, The Journal of Physical Chemistry C 123 (2019) 19704–19714, https://doi.org/10.1021/acs.jpcc.9b05363.

[30] J.L.S. Lee, I.S. Gilmore, M.P. Seah, A.P. Levick, A.G. Shard, Topography and field effects in secondary ion mass spectrometry Part II: insulating samples, Surf. Interface Anal. 44 (2012) 238–245, https://doi.org/10.1002/sia.3833.

[31] S. Rangarajan, B.J. Tyler, Topography in secondary ion mass spectroscopy images, J. Vac. Sci. Technol., A 24 (2006) 1730–1736, https://doi.org/10.1116/1.2217980.

[32] H. Tian, D. Maciążek, Z. Postawa, B.J. Garrison, N. Winograd, C-O bond dissociation and induced chemical ionization using high energy $(CO_2)_n^+$ gas cluster ion beam, J. Am. Soc. Mass Spectrom. 30 (2019) 476–481, https://doi.org/10.1007/s13361-018-2102-z.

[33] M.F. Drumm, C.W.H. Dodge, L.E. Nielsen, Cross linking of a phenol-formaldehyde novolac - determiantion by dynamic-mechanical measurements, Ind. Eng. Chem. 48 (1956) 76–81, https://doi.org/10.1021/ie50553a026.

[34] J.B. Enns, J.K. Gillham, Torsional Braid Analysis, in: Polymer Characterization, American Chemical Society, 1983, pp. 27-63.

[35] P. Gradin, G.P. Howgate, R. Selden, A.R. Brown, Dynamic-mechanical proprties, in: G. Allen, J.C. Bevington (Eds.), Comprehensive Polymer Science and Supplements, Pergamon Press, New York, 1989, pp. 533–569.